

Typhoon – Ocean Interactions Inferred by Multi-Sensor Observations

I-I Lin and Chun-Chieh Wu

Dept. of Atmospheric Sciences, National Taiwan University, Taipei, Taiwan

August 30, 2007

Corresponding author address: Dr. I-I Lin, Dept. of Atmospheric Sciences, National Taiwan University, No. 1, Sec. 4, Roosevelt Rd., Taipei 106, Taiwan; e-mail: iilin@webmail.as.ntu.edu.tw

Abstract

The Western North Pacific Ocean and surrounding Seas are among the world's oceans where tropical cyclones, both highest in number and intensity, are found. Since there has long been interest in studying the typhoon-ocean interaction processes in this vast oceanic region. However, observations are rare and it has been difficult to study these complex, dynamic, and interdisciplinary processes. With the advancement in satellite remote sensing, especially in microwave remote sensing with cloud-penetrating capabilities, it has finally become possible to catch a glimpse into some of these processes in the western North Pacific. In this paper, we review a number of recent papers using these new satellite observations to study (1) the interaction between typhoons and warm ocean eddies, (2) enhancement in ocean primary production induced by typhoons, and (3) post-typhoon air-sea interaction.

1. Introduction

The interaction between tropical cyclones and the ocean is complex, dynamic, and interdisciplinary. Tropical cyclones form on the ocean, which is the energy source that fuels a cyclone's intensification (Emanuel 1986; 1988; 1991; 1995; Holland 1997; Black et al. 2007). As cyclones intensify, they impact back to the ocean and cause cold water from the deeper ocean to be entrained and upwelled to the upper ocean layer (Chang and Anthes 1979; Price 1981; Stramma et al. 1986; Shay et al. 1992; Dickey et al. 1998; Jacob et al. 2000). This self-induced ocean cooling in turn plays a critical negative feedback role in the cyclone's intensification (Gallacher et al. 1989; Emanuel 1999; Schade and Emanuel 1999; Bender and Ginis 2000; Cione and Uhlhorn 2003; Emanuel et al. 2004; Lin et al. 2005; Zhu and Zhang 2006; Wu et al. 2007). After the cyclones' departure, cold wakes, typically more evident to the right of the cyclone tracks (Change and Anthes 1978; Price 1981; Cornillon et al. 1987; Bender and Ginis 2000; Monaldo et al. 1997; Wentz et al. 2000; Lin et al. 2003b) are left behind. These cold wakes can exist in the ocean for days to weeks and generate continual feedback with the atmosphere (Emanuel 2001; Lin et al. 2003a).

Besides the above physical interactions, there can also be biogeochemical interactions between cyclones and the ocean because the intense cyclone wind not only mixes and transports the cold water from the deeper ocean but also nutrients in the deeper layer (Lin et al. 2003b; Babin et al. 2004; Davis and Yan 2004; Siswanto et al. 2007). As most of the tropical and subtropical oceans are oligotrophic, i.e., nutrient-poor (Eppley 1989; Behrenfeld and Falkowski, 1997; McGillicuddy et al. 1998; McGillicuddy et al. 2001; Uz et al. 2001), the nutrients brought to the upper ocean are critical for phytoplankton, inducing phytoplankton blooms (Lin et al. 2003b; Babin et al. 2004; Siswanto et al. 2007). Also, since phytoplankton is the base of the marine food chain, these blooms may produce a chain reaction to affect the fishery yield. This phenomenon has not been lost to experienced fishermen who harvest in the wake long after a tropical cyclone's passage. Besides being the base of the ocean food chain, these phytoplankton blooms can have even more profound impact to the earthy

system. Like all other plants, phytoplankton uses carbon dioxide, sunlight and nutrients to photosynthesize; additionally, half of the world's oxygen is produced by phytoplankton. Therefore, phytoplankton production also affects the uptake of carbon dioxide, an important greenhouse gas and a major cause of natural and man-made climate changes (Eppley and Peterson 1979; Eppley 1989; Bates et al. 1998; McGillicuddy et al. 1998; Lin et al. 2003b; Uz et al. 2001).

Pre-existing ocean features are known to cause even more complex air-sea interactions in the tropical cyclone and ocean system (Qiu 1999; Shay et al. 2000; Goni and Trinanes 2003; Emanuel et al. 2004; Lin et al. 2005; Scharroo et al. 2005; Oey et al. 2007; Wu et al. 2007). It has been reported that some major category-5¹ storms, e.g., Hurricane Opal of 1995 (Shay et al. 2000), Katrina of 2005 (Scharroo et al. 2005), super-typhoon Maemi of 2003 (Lin et al. 2005), and Dianmu of 2004 (Pun et al. 2007) rapidly intensified when encountering warm ocean features.

Western North Pacific Basin and the surrounding seas are where most tropical cyclone (i.e., typhoon) activities are located. But due to the lack of *in situ* and airborne observations, it has been difficult to credibly analyze the complex typhoon-ocean interaction processes in this basin. Available opportune *in situ* observations in this region are too sparse to lend meaningful spatial correlations. Visible and IR satellite remote sensing images (e.g., Advanced Very High Resolution Radiometer, AVHRR) are frequently contaminated by clouds (Wentz et al. 2000), especially near typhoons, limiting the usefulness of these images for our purposes. Therefore, observations of typhoon-ocean interactions in the north Western Pacific have been extremely difficult. With recent advancements in microwave remote sensing (Fu et al. 1994; Fu and Cazenave 2001; Liu et al. 1998; Wentz et al. 2000), however, some inroads have been made in exploring the processes that occur at the air-sea interface as typhoons translate over the ocean.

¹ Saffir-Simpson Tropical Cyclone Scale based on the 1-minute maximum sustained winds: Category-1: 34-43 ms⁻¹, Category-2: 44-50 ms⁻¹, Category-3: 51-59 ms⁻¹, Category-4: 59-71 ms⁻¹, and Category-5: > 71 ms⁻¹.

The major advantage to using microwave remote sensing is its ability to penetrate clouds and its independence of sunlight. Therefore, observations can be made both day and night without bias to fair-weather at the air-sea interface. For the 50th anniversary of the Department of Atmospheric Sciences of National Taiwan University, we demonstrate in this review the use of three types of microwave remote sensors and one optical remote sensor to study a number of -little-studied or infrequently-observed typhoon-ocean interaction processes in the western North Pacific based on a series of recent papers (Lin et al. 2003a; Lin et al. 2003b; Lin et al. 2005). The three types of microwave data are 1) the ocean surface wind vector from the QuikSCAT active microwave scatterometer (Liu et al. 1998), 2) the sea surface temperature (SST) data from the TRMM (Tropical Rainfall Measuring Mission) passive microwave imager and the Advanced Microwave Scanning Radiometer (AMSR-E) (Wentz et al. 2000), and 3) the sea surface height anomaly (SSHA) data from the TOPEX-Poseidon and JASON-1 active microwave altimeters (Fu et al. 1994; Fu and Cazenave 2001). The optical remote sensor used is the ocean color data from the NASA Sea-viewing Wide Field-of-view (SeaWiFS) sensor (O'Reilly et al. 1998). In this work, the QuikSCAT, TOPEX-Poseidon, and JASON-1 data are from the daily level-2 product of the NASA/Jet Propulsion Laboratory. The SeaWiFS data is the daily level-2 chlorophyll-a data of the NASA Goddard Space Flight Center while the TRMM/SST data is the daily product of the Remote Sensing Systems (Wentz et al. 2000). All products have been validated with *in situ* observations and the readers are referred to the original references (Fu et al. 1994; Liu et al. 1998; O'Reilly et al. 1998; Wentz et al. 2000) for their respective accuracies.

In Section 2, we will discuss the interaction between super-typhoon Maemi (2003) and a warm ocean eddy (Lin et al. 2005), and show that warm ocean eddies play a critical role in Maemi's intensification to category-5. In Section 3, we will show the drastic biological response induced by typhoon Kai-Tak (2000) in the South China Sea (Lin et al. 2003b). In Section 4, we present observations in previously-unobserved post-typhoon air-sea interaction processes that the cold wakes, left behind by typhoons, can have evident feedback to the atmosphere by reducing the ocean surface

wind speed (Lin et al. 2003a). In section 5, a summary is presented.

2. The interaction of supertyphoon Maemi (2003) and a warm ocean eddy (based on Lin et al., 2005)

Since the observation of a noticeable number of intense category-4 or 5 Atlantic/Gulf of Mexico hurricanes (e.g., Opal (1995), Mitch (1998), Bret (1999)) rapidly intensified to category-5 when encountering warm mesoscale ocean eddies (Shay et al. 2000; Goni and Trinanes 2003; Emanuel et al. 2004), there is much interest in studying the interaction between tropical cyclones and ocean features (e.g., eddies and currents) (Shay et al. 2000; Hong et al. 2000; Goni and Trinanes 2003; Emanuel et al. 2004; Lin et al. 2005; Scharroo et al. 2005; Oey et al. 2006; Pun et al. 2007; Wu et al. 2007). In particular, it is suggested that the warm eddy in the Gulf of Mexico may have induced the intensification of the devastating Hurricane Katrina of 2005 to category-5 before its landfall (Scharroo et al. 2005). The Western North Pacific Ocean is among the world's oceans in which the greatest number of intense category-4 and 5 cyclones are found². It is interesting to find out whether these intense typhoons are associated with ocean features. In this section, we review the first event observed in the western North Pacific of such an encountering.

In September 2003, typhoon Maemi passed directly over a prominent warm ocean eddy in the western North Pacific, as observed by the satellite SSHA data from the TOPEX/Poseidon and JASON-1 altimeters (Fu et al. 1994). This warm ocean eddy is around 700km × 500km in size and is characterized by its large positive SSHA³ of 10-45cm (Fig. 1). Joint-analysis with the best track data from the Joint Typhoon Warning Center (JTWC) shows that during the 36 h of the Maemi-eddy encountering, Maemi's intensity (in 1-min sustained wind) shot up from the modest category-1 (41 m

² From the best track data of the best-track data of Joint Typhoon Warning Center during 1960-2005.

³ From existing literature, warm ocean features with SSHA > 8cm is considered as prominent. (Qiu, 1999; Shay et al. 2000).

s^{-1}) to its peak in category-5 (77 m s^{-1}). As can be observed in Fig. 1, Maemi entered into the eddy region at 1800 UTC 8 September 2003 when its intensity was at category-1 (green bullet). It then rapidly intensify to category-2, (blue bullet) in 6h and jumped to category-4 (i.e., yellow bullet) in the next 6h. At 0000UTC 10 September, 2003 (i.e., 36h from category-1), Maemi reached its peak at category-5 (77 m s^{-1} , black bullet) and became the most intense tropical cyclone globally in 2003. As Maemi left the eddy region, its intensity declined.

Using a simple coupled typhoon-ocean model, i.e., the CHIPS (Coupled Hurricane Intensity Prediction System) model (Emanuel 1999; Emanuel et al. 2004), numerical experiments were conducted to assess the influence of the warm eddy on the intensity evolution of Maemi. Numerical experiments are run with and without the input of the eddy information derived from the satellite SSHA field. The run without the eddy input (denoted as CTRL) uses monthly climatological ocean mixed layer depth (Levitus 1982). The one with the eddy input (denoted as EDDY) uses 1 cycle (10 days) of the observed pre-typhoon satellite SSHA measurement as input to an algorithm developed by Shay et al. (2000) to estimate a new mixed layer depth (Emanuel et al. 2004) (Fig. 2). The best-track intensity data from the JTWC is also shown in Fig. 2a. All the runs were initialized and tuned according to the best-track data for the first 24 h.

As in Fig. 2a, it is evident that the intensity evolutions, including the eddy-adjusted mixed-layer depth, are much closer to the best track intensity than the run without the eddy (i.e., CTRL) in both the magnitude and timing of the peak intensity. The peak intensity is 68 m s^{-1} (i.e., category-4) for the CTRL run, but the observed peak is 77 m s^{-1} , occurring at 0300 UTC 10 September (Fig. 2a). Maemi reaches its maximum intensity in CTRL at 1800 UTC 9 September, 9 h earlier than the OBS. When the warm eddy is included to initialize a deeper mixed-layer in CHIPS, an improvement in intensity hindcast is evident. The peak intensity for the EDDY run reaches the category-5 scale of 75 m s^{-1} , well-matched by the observed best-track intensity peak. The timing for peak intensity is also correctly captured (Fig. 2a).

Further analysis of the CHIPS results find that the reason why the EDDY run can match well

with the observed intensity is because the upper ocean thermal structure in the warm eddy is correctly represented by the satellite SSHA in the EDDY run. As can be seen in Fig. 3, in the eddy region, warm water of 26°C well extends downward to about 120-130m. In contrast, outside the eddy region the subsurface warm layer is much shallower, so that the warm water of 26°C extends only to 40m or so (i.e., background). Also, it is noted that the difference between eddy and the background is not in SST, but in the subsurface thermal structure. As can be seen in Fig. 3, both background and eddy profiles show similar SST values of around 28.2°C . In other words, what makes the difference is the thickness of the subsurface warm layer, but not the SST.

Fig. 2b shows that with the very deep warm mixed layer in the warm eddy, typhoon-induced ocean surface cooling is significantly suppressed. The typhoon-induced ocean cooling is only $\leq 0.5^{\circ}\text{C}$ (red curve in Fig.2b) throughout the intensification period before the storm reaches peak intensity at 0300 UTC 10 September. As a consequence, the storm is able to intensify without being hampered by the cooler sea surface temperature induced by the typhoon, as the negative feedback mechanism (Emanuel 1999, Bender and Ginis 2000, Emanuel et al. 2004) is reduced in the presence of the warm eddy. In contrast, in the CTRL run (green curve), the self-induced ocean cooling is much stronger with SST anomaly $\sim 1.5\text{-}2.5^{\circ}\text{C}$ (Fig. 2b) during the intensification period (0000 UTC 5 September to the peak at 0300 UTC 10 September) without the warm eddy and its deep warm mixed layer. The increased cooling of the sea surface in the CTRL experiment contributes to the reduction of maximum wind speed by $\sim 10\text{ m s}^{-1}$ of the simulated storm as evident in Fig 2a (green curve).

In the current literature, three other cyclone-warm ocean feature interaction cases in the Atlantic (i.e., Hurricanes Opal, Mitch, and Bret) have been studied using atmosphere-ocean coupled models (Hong et al. 2000; Emanuel et al. 2004). Opal (1995) was simulated in Hong et al. (2000) using the U.S. Naval Research Laboratory's Coupled Ocean-Atmosphere Mesoscale Prediction System (COAMPS) as the atmospheric component and the Geophysical Fluid Dynamics Laboratory's

Modular Ocean Model version 2 (MOM2) as the ocean component. The other two cases, Mitch (1998) and Bret (1999), were run using the CHIPS model (Emanuel et al. 2004). Table 1 compares the results of these 3 Atlantic cases with the Maemi case.

In Table 1, it is clear that in all cases without the warm ocean eddy information, the intensity is too low as compared to the best track intensity. With the addition of the eddy information in the numerical experiments, the predicted intensity is evidently improved. In the case of Opal, the peak of the without-eddy simulation reaches only to category-4 (i.e., 932 hPa). When the eddy is included, the peak intensity reaches 916hPa, in agreement with the best track peak at category-5 (Hong et al. 2000). Consistent results are also found in Mitch, Bret, and Maemi: without the inclusion of the ocean feature in the simulation, intensity is about 26-31% lower (typically 1 category lower) as compared to the best track peak (Table 1). With the inclusion of the eddy information in the simulation, the peak intensity can be correctly-simulated (Table 1).

3. Ocean's biogeochemical response to typhoon (based on Lin et al., 2003b)

When passing over land, tropical cyclones can affect human lives and activities. Over the ocean, they can also affect other form of life, i.e., the ocean primary production. As introduced in Section 1, ocean primary production plays a significant role in the earth ecological and environmental system, especially because it affects the uptake of the important greenhouse gas, carbon dioxide (Eppley and Peterson 1979; Eppley 1989; Behrenfeld and Falkowski 1997; Bates et al. 1998; McGillicuddy et al. 1998; Uz et al. 2001; Babin et al. 2004). Primary production takes place mainly in the euphotic zone of the ocean, i.e., the top 50 to 150 m of the water column where there is abundant light for photosynthesis and when nutrients are available. Marine nutrients, however, are mostly located in the deeper ocean. Therefore, the vertical entrainment due to mixing and the induced upwelling in the ocean, caused by tropical cyclone winds, are crucial mechanisms in the earth system that the deep, cold, nutrient-rich water can be brought up from the deeper layer to the light-replete euphotic zone.

The nutrients can then fuel photosynthetic activities and cause enhancement in primary production (i.e., phytoplankton bloom) (Eppley 1989; Marra et al. 1990; Dickey et al. 1998; Lin et al. 2003b). Such processes are difficult to monitor and measure, and a quantitative determination of the change of the marine primary production induced by tropical cyclones is elusive.

During the three days from 5 to 8 July 2000 that Typhoon Kai-Tak translated over the South China Sea, it triggered a huge phytoplankton bloom with an average of a 30 times-over increase in surface chlorophyll-a (Chl-a) concentration, as observed by the SeaWiFS (O'Reilly et al. 1998) sensor. In this Section, major findings of this event based on Lin et al. 2003b are introduced. This is one the first quantitative events documenting such a typhoon-induced biogeochemical response in the western North Pacific and adjacent Seas.

Kai-Tak was a moderate Category-2 typhoon in the Saffir-Simpson hurricane scale. It lingered at a nearly stationary slow speed of $0-1.4 \text{ ms}^{-1}$ on the northern South China Sea (from 5 to 8 July 2000 before it proceeded speedily ($\sim 6.1 \text{ ms}^{-1}$) northwards thereafter (Fig. 4b). The biological response to the passing of Kai-Tak was depicted by changes in the surface distribution of Chl-a. The pre-typhoon condition was illustrated in the SeaWiFS composite from 27 June - 4 July 2000 (Fig. 4a), which showed the typical summer surface Chl-a concentrations of predominantly $\leq 0.1 \text{ mgm}^{-3}$. After Kai-Tak's passage (5-8 July), the first available cloud-free SeaWiFS image composite (12-15 July) illustrated an evident enhancement of biological activity, as revealed by the Chl-a concentration (Fig. 4b). The bloom patch ($117.5-120^\circ\text{E}$, $19.3-20.7^\circ\text{N}$), predominantly of Chl-a concentrations around 10 mgm^{-3} , coincided with Kai-Tak's trajectory and its radius of intense wind ($\sim 14 \text{ ms}^{-1}$). At certain locations (e.g. 118.4°E , 20°N), the Chl-a concentrations reached as high as 30 mgm^{-3} , 300 fold of the pre-typhoon condition as depicted in the Chl-a distribution (in log scale) along tr1 (Fig. 4c). The pre-typhoon (from Fig. 4a) and the 3-year (1998, 1999, and 2001) monthly average of July Chl-a concentrations along tr1 are also depicted for comparison in Fig. 4c.

Another drastic response can be observed in Fig. 5 is the drop in SST. Before Kai-Tak's arrival, the SCS was characterised by a warm SST predominantly above 30°C (Fig.5a). Immediately after Kai-Tak's departure, on 9 July, a cold SST (21.5-24°C) pool (118-120°E, 19-20.5°N) of size comparable to Kai-Tak's 150-km radius of intense wind (14 ms^{-1}), co-located with the typhoon's track was observed (Fig. 5b). The minimum SST of 21.5°C was found at the centre (118.9°E, 19.9°N) of the cold pool. In comparison with the pre-typhoon condition (30.7°C), the SST dropped as much as 9°C. The distributions of SSTs along the cross-section tr1 (depicted in Fig. 5) over the cold pool before and after the passing of the typhoon, and the 3-year (1998, 1999, and 2001) mean for July are shown in Fig. 5c. Since the 1960s, there have been a number of observational and modelling studies on typhoon-induced upper ocean cooling responses (Chang and Anthes 1978; Price 1981; Stramma et al. 1986; Cornillon et al. 1987; Monaldo et al. 1997; Dickey et al. 1998; Bender and Ginis, 2000; Wentz et al. 2000) with reported SST reduction generally spanning 0.5-6°C. The 9°C cooling inferred by TRMM microwave imager here is one of the strongest ever observed. In the original paper (Lin et al. 2003b), entrainment mixing and upwelling velocity are estimated to show that due to the shallow thermocline in the South China Sea during summer, it is possible for a near-stationary typhoon to induce such a drastic cooling response.

Using the observed Chl-a and SST data as input to a marine primary production model (Behrenfeld and Falkowski 1997), it is possible to estimate the contribution of Kai-Tak to marine primary production. The changes in SST, surface Chl-a, and depth-Integrated Primary Production (IPP) with time at the center of the phytoplankton bloom (Lin et al. 2003b) are shown in Fig. 6. The temperature depression and the phytoplankton bloom, as indicated by the elevation of Chl-a concentration, could be tracked for about 1 month. The pre-typhoon IPP was $300 \text{ mg C m}^{-2} \text{ d}^{-1}$, similar to the annual mean (Liu et al. 2002) IPP of $350 \text{ mg C m}^{-2} \text{ d}^{-1}$. After the passage of the typhoon, IPP increased almost an order of magnitude to $2800 \text{ mg C m}^{-2} \text{ d}^{-1}$. By integrating IPP over the bloom patch through each time interval, the carbon fixation resulting from this single event (12

July-16 August) was about 0.8 Mt ($1\text{Mt} = 10^{12}\text{g}$) of carbon. Taking the 200m bathymetry as the lower boundary of the oligotrophic waters, the area of the oligotrophic South China Sea is $2.76 \times 10^6 \text{ km}^2$, or about 80% of the total area of the South China Sea. If the f ratio in the South China Sea is similar to those in other oligotrophic waters, 0.06 to 0.14 (Eppley 1989), Typhoon Kai-Tak would have accounted for 2 to 4 % of the annual marine primary production in the oligotrophic South China Sea⁴.

Due to the lack of definitive observations, the contribution of tropical cyclones to primary production has long been treated as negligible. Our result, based on the synergy of three recently-available satellite data sets, proves, on the contrary, that tropical cyclones induce significant contribution to the overall primary production in tropical seas.

4. Post typhoon air-sea interaction (based on Lin et al., 2003a)

As discussed before, tropical cyclones can cool the ocean surface and mixed layer by induced entrainment and upwelling as deep, cold water is brought to the upper ocean layer. After a typhoon's departure, a cold wake is left behind. As in Section 3, the cold patches in the wake may be as much as 9°C cooler than the surrounding warm ocean (Lin et al. 2003b). Therefore they represent a sizable perturbation of the SST in an otherwise relatively uniform warm ocean environment. This presents a unique natural laboratory to investigate the nature of ocean-atmospheric coupling.

Followed from Section 3, the case of typhoon Kai-Tak is chosen to study the post-typhoon air-sea interaction. In this work, co-located and near co-incident TRMM SST and QuikSCAT wind vectors are inter-compared. It can be observed in Fig. 7a that prior to Kai-Tak, the northern South China Sea was under typical summer conditions with SST in the range of $30.5\text{-}33.0^\circ\text{C}$. The corresponding wind field (Fig. 8a) is characterized by higher wind speed (9-11 m/s) at the region

⁴ The oligotrophic part of the South China Sea in this work is defined as the basin (i.e., open ocean part) of the South China Sea where the bathymetry is typically $> 200\text{m}$.

north of 19°N, while south of 19°N, wind speed is lower (range between 3-6 m/s). No evident association between SST and wind is observed. Between 5-8 July, Kai-Tak passed over the South China Sea (Fig. 7b). Though the maximum SST cooling occurred on 9 July (as introduced in Section 3 and Fig. 4b), the wind fields were still then under the influence of the typhoon. Post-typhoon response is studied from 11 July onwards. From Figure 7b, one sees that the cold SST patch (118-120°E, 19-21°N) has the dimension of around 150-200 km and the minimum SST of 22°C is found (color coded: purple) in the centre (118.9°E, 19.9°N) of the oval cold patch and increases outwards to 26°C (light blue) towards the edge. The surrounding SST is around 29-30°C (dark-light green). The corresponding wind field (Fig. 8b) shows a distinctive minimum spatially co-incident with the cold patch. The wind speed inside the cold patch is between 2.5 to 6ms⁻¹ (dark purple-light blue) while the surrounding wind speed is between 8-11 ms⁻¹ (green-yellow color).

Observing Fig. 7c/8c, Fig. 7d/8d, and Fig. 7e/8e, similar correlation between the cold SST patch and reduction in wind speed can be found till 19 July, persisting for eight days. For example, on 13 July, the induced cold SST pattern had weakened and elongated (Fig. 7d), but the corresponding wind speed (Fig. 8d) evolved into similar shapes, illustrating the close-correlation between SST and wind with relatively high (≥ 12 m/s) wind north and south of the cold patch. This again shows that the wind speed over the cold SST patch remains relatively low, in contrast to the high wind in the adjacent areas to the north and south of it. On 19 July, the cold patch has much diminished into a small circular feature at around 117.5°E, 20°N (Fig. 7e), and disappears shortly thereafter. This is consistent with the mechanism proposed by Wallace et al. (1989), that cool SST is correlated to low surface wind because of a decrease of atmospheric boundary layer stability. Over colder waters, the marine boundary layer is stable, vertical mixing is suppressed, and vertical wind shear increases, the surface wind speed is reduced.

In the existing literature, a number of studies report similar correlation between SST and surface wind speed under a much longer time (~20-40days) and spatial scale (~ 1000-2000 km), i.e., in the

case of Tropical Instability Waves and the Eastern Pacific Ocean cold tongue (Xie et al. 1998; Wentz et al. 2000; and Chelton et al. 2001). Our results supports the Wallace et al. (1989) hypothesis in the SST-wind coupling in a different situation, namely in the cold SST wakes of typhoons. What we show in our examples discussed above are the small space and short time scales over which this mechanism can act. In the typhoon-induced cold wake situation, the coupling manifests itself within a day and of the spatial scale of 100-400km. In the original paper (Lin et al. 2003a), the relationship between wind speed and SST anomalies is further investigated. Also, similar correlation between wind and SST in the cold wake of supertyphoon Bilis (2000) is found. Interested readers are referred to Lin et al. (2003a) for further details.

5. Summary

In this review, we introduced applications of new satellite observations of previously rarely-observed typhoon-ocean interaction phenomena in the western North Pacific and adjacent Seas, as been published in Lin et al. (2003a, b, 2005). Examples for three different phenomena are presented to illustrate, the interaction between typhoon and warm ocean eddy, enhancement in ocean primary production induced by typhoon, and post-typhoon air-sea interaction. These new observations show that:

1. The presence of warm ocean eddies plays a critical role in super-typhoon Maemi's intensification. In the presence of a warm ocean eddy with deep warm ocean water, typhoon self-induced ocean cooling is much reduced. As a result, Maemi (2003) was able to reach Category-5, due to the minimal negative feedback. Numerical experiments by the CHIPS (Emanuel 1999; Emanuel et al. 2004) coupled typhoon-ocean model finds that without the presence of warm ocean eddy, Maemi's intensity could only reach category-4.
2. Typhoons can induce drastic biological responses in the ocean, and hence may play a

significant role in the marine primary production and carbon fixation. As observed in the case of typhoon Kai-Tak (2000), during its short three-day meandering in the South China Sea, this moderate category-2 typhoon caused an average of 30-fold increase in ocean surface chlorophyll-a concentration. The estimated carbon fixation resulting from this event alone is 0.8 Mt, or 2-4% of South China Sea's annual new production. Each year, about 14 cyclones pass over the South China Sea, suggesting that the long-neglected contribution of typhoons to South China Sea's annual new production may be as much as 20-30%.

3. There is an interesting air-sea coupling long after typhoon's passage. The cold wake left behind by the typhoon existed for more than a week, as observed in the case of typhoon Kai-Tak (2000). Inter-comparison of co-incident/co-located QuikSCAT ocean surface wind vectors finds clear and consistent weakening of the surface wind speed over the cold SST wake. This suggests that the boundary layer stability is increased because of the cold ocean surface, and the surface wind speed is reduced due to diminished vertical mixing (Wallace et al. 1989; Xie et al. 1998; Chelton et al. 2001). In particular, our result suggests that this mechanism can act on relatively small spatial (~100km) and short (~1 day) time scale, as contrast to the previously reported much longer time (~20-40days) and large spatial scale of ~ 1000-2000km (Xie et al. 1998; Wentz et al. 2000; Chelton et al. 2001).

As the above works are based on studies of an individual case' ongoing efforts are being made to conduct systematic analysis in studying the typhoon-ocean interaction problems in the western North Pacific.

References

Babin, S. M., J. A. Carton, T. D. Dickey, and J. D. Wiggert, 2004: Satellite evidence of

hurricane-induced phytoplankton blooms in an oceanic desert. *J. Geophys. Res.*, 109, C03043, doi:10.1029/2003JC001938.

Bates, N. R., A. H. Knap, and A. F. Michaels, 1998: Contribution of hurricanes to local and global estimates of air-sea exchange of CO₂, *Nature*, 395, 58-61.

Behrenfeld, M. J., and P. G. Falkowski, 1997: Photosynthetic rates derived from satellite based chlorophyll concentration. *Limnology and Oceanography*, 42, 1-20.

Bender, M. A., and I. Ginis, 2000: Real-case simulations of hurricane–ocean interaction using a high-resolution coupled model: Effects on hurricane intensity. *Mon. Wea. Rev.*, 128, 917–946.

Black, P. G., E. A. D'Asaro, W. M. Drennan, J. R. French, P. P. Niller, T. B. Sanford, E. J. Terrill, E. J. Walsh, and J. A. Zhang, 2007: Air-sea exchange in hurricanes, synthesis of observations from the Coupled Boundary Layer Air-Sea Transfer Experiment. *Bull. Amer. Meteor. Soc.*, 88, 357-374.

Chang, S. W. and R. A. Anthes, 1978: Numerical simulations of the ocean's nonlinear, baroclinic response to translating hurricanes. *J. Phys. Oceanogr.*, 8, 468-480

Chang, S. W. and R. A. Anthes, 1979: The mutual response of the tropical cyclone and the ocean. *J. Phys. Oceanogr.*, 9, 128-135.

Chelton, D. B., S. K. Esbensen, M. G. Schlax, N. Thum, M. H. Freilich, F. J. Wentz, C. Gentemann, M. J. McPhaden, and P. S. Schopf 2001: Observations of coupling between surface wind stress and sea surface temperature in the Eastern Tropical Pacific. *J. Climate*, 14, 1470–1498.

Cione, J. J., and E. W. Uhlhorn, 2003: Sea surface temperature variability in hurricanes: Implications with respect to intensity change. *Mon. Wea. Rev.*, 131, 1783–1796.

Cornillon, P., L. Stramma, and J. F. Price, 1987: Satellite measurements of sea surface cooling during hurricane Gloria. *Nature*, 326, 373-375.

Davis, A., and X. H. Yan, 2004: Hurricane forcing on chlorophyll-a concentration off the northeast coast of the U.S., *Geophys. Res. Lett.*, 31, L17304, doi: 10.1029/2004GL020668.

Dickey, T., D. Frye, J. McNeil, D. Manov, N. Nelson, D. Sigurdson, H. Jannasch, D. Siegel, A.

- Michaels, and R. Johnson, 1998: Upper-ocean temperature response to Hurricane Felix as measured by the Bermuda Testbed Mooring. *Mon. Wea. Rev.*, 126, 1195–1201.
- Emanuel, K. A., 1986: An air-sea interaction theory for tropical cyclones Part I. *J. Atmos. Sci.*, 42, 1062–1071.
- Emanuel, K. A., 1988: The maximum intensity of hurricanes. *J. Atmos. Sci.*, 45, 1143–1155.
- Emanuel, K.A., 1991: The theory of hurricanes. *Annual Rev. Fluid Mech.*, 23, 179-196.
- Emanuel, K. A., 1995: Sensitivity of tropical cyclones to surface exchange coefficients and a revised steady-state model incorporating eye dynamics. *J. Atmos. Sci.*, 52, 3969–3976.
- Emanuel, K. A., 1999: Thermodynamic control of hurricane intensity. *Nature*, 401, 665–669.
- Emanuel, K.A., 2001: The contribution of tropical cyclones to the oceans' meridional heat transport. *J. Geophys. Res.*, 106, 14771-14781.
- Emanuel, K. A., C. DesAutels, C. Holloway, and R. Korty, 2004: Environmental control of tropical cyclone intensity. *J. Atmos. Sci.*, 61, 843–858.
- Eppley, R. W., and B. J. Peterson, 1979: Particulate organic matter flux and planktonic new production in the deep ocean. *Nature*, 282, 677–680.
- Eppley, R. W., 1989: New production: History, methods, problems. *Productivity of the Ocean: Present and Past*, edited by W. H. Berger, V. S. Smetacek, and G. Wefer, Wiley, Chichester, 85–97.
- Fu, L. L., E. J. Christensen, C. A. Yamarone, M. Lefebvre, Y. Menard, M. Dorrer, and P. Escudier, 1994: TOPEX/POSEIDON mission overview. *J. Geophys. Res.*, 99, 24369–24381.
- Fu, L. L. and A. Cazenave, 2001: *Satellite Altimetry and Earth Sciences, A Handbook of Techniques and Applications*, *International Geophysics Series*, 69, Academic Press, San Diego.
- Gallacher, P. C., R. Rotunno, and K. A. Emanuel, 1989: Tropical cyclogenesis in a coupled ocean–atmosphere model. Preprints, *18th Conf. on Hurricanes and Tropical Meteorology*, San Diego, CA, Amer. Meteor. Soc., 121–122.
- Goni, G. J., and J. A. Trinanes, 2003: Ocean thermal structure monitoring could aid in the intensity

- forecast of tropical cyclones. *Eos, Trans. Amer. Geophys. Union*, 84, 573–580.
- Holland, G. J., 1997: The maximum potential intensity of tropical cyclones. *J. Atmos. Sci.*, 54, 2519–2541.
- Hong, X., S. W. Chang, S. Raman, L. K. Shay, and R. Hodur, 2000: The interaction between Hurricane Opal (1995) and a warm core eddy in the Gulf of Mexico. *Mon. Wea. Rev.*, **128**, 1347-1365.
- Jacob, S. D., L. K. Shay, A. J. Mariano, and P. G. Black, 2000: The 3-D oceanic mixed layer response to hurricane Gilbert. *J. Phys. Oceanogr.*, 30, 1407-1429.
- Ko, D. S., R. H. Preller, G. A. Jacobs, T. Y. Tang, and S. F. Lin, 2003: Transport reversals at Taiwan Strait during October and November 1999. *J. Geophys. Res.*, 108, C11, 3370.
- Levitus, S., 1982: *Climatological Atlas of the World Ocean*. NOAA Prof. Paper 13, 173 pp. and 17 microfiche.
- Lin, I. I., W. T. Liu, C. C. Wu, J. C. H. Chiang, and C. H. Sui, 2003: Satellite observation of Modulation of surface Layer Winds by Typhoon-Induced Upper Ocean Cooling. *Geophys. Res. Lett.*, 30, 1131, doi:10.1029/2002GL015674.
- Lin, I. I., W. T. Liu, C. C. Wu, G. T. F. Wong, C. Hu, Z. Chen, W. D. Liang, Y. Yang, and K. K. Liu, 2003: New evidence for enhanced ocean primary production triggered by tropical cyclone. *Geophys. Res. Lett.*, 30, 1718, doi:10.1029/2003GL017141.
- Lin, I. I., C. C. Wu, K. A. Emanuel, I. H. Lee, C. R. Wu, and I. F. Pun, 2005: The Interaction of Supertyphoon Maemi (2003) With a Warm Ocean Eddy. *Mon. Wea. Rev.* 133, 2635-2649.
- Liu, K. K., S. Y. Chao, P. T. Shaw, G. C. Gong, C. C. Chen, and T. Y. Tang, 2002: Monsoon-forced chlorophyll distribution and primary production in the South China Sea. *Deep-Sea Res., Part I*, 49, 1387-1412.
- Liu, W. T., W. Tang, and P. Polito, 1998: NASA scatterometer provides global ocean-surface wind fields with more structures than numerical weather prediction. *Geophys. Res. Lett.*, 25, 761–764.

- Marra, J., R. R. Bidigare, and T. D. Dickey, 1990: Nutrients and mixing, chlorophyll and phytoplankton growth. *Deep-Sea Res.*, 37, 127–143.
- McGillicuddy, D. J., A. R. Robinson, D. A. Siegel, H. W. Jannasch, R. Johnson, T. D. Dickey, J. McNeil, A. F. Michaels, and A. H. Knap, 1998: Influence of mesoscale eddies on new production in the Sargasso Sea. *Nature*, 394, 263–266.
- McGillicuddy, D. J., V. K. Kosnyrev, J. P. Ryan, and J. A. Yoder, 2001: Covariation of mesoscale ocean color and sea-surface temperature patterns in the Sargasso Sea, *Deep Sea Res., Part II*, 48, 1823-1836.
- Monaldo, F. M., T. D. Sikora, S. M. Babin, and R. E. Sterner, 1997: Satellite imagery of sea surface temperature cooling in the wake of hurricane Edouard (1996). *Mon. Weather Rev.*, 125, 2716-2721.
- Oey, L. Y., T. Ezer, D. P. Wang, X. Q. Yin, and S. J. Fan, 2007: Hurricane-induced motions and interaction with ocean currents. *Cont. Shelf Res.*, 27, 1249-1263.
- O'Reilly, J. E., S. Maritorena, B. G. Mitchell, D. A. Siegel, K. L. Carder, S. A. Garver, M. Kahru, and C. McClain, 1998: Ocean color chlorophyll algorithms for SeaWiFS. *J. Geophys. Res.*, 103, 24937– 24953.
- Price, J. F., 1981: Upper ocean response to a hurricane. *J. Phys. Oceanogr.*, 11, 153– 175.
- Pun, I. F., I. I. Lin, C. R. Wu, D. S. Ko, and W. T. Liu, 2007: Validation and Application of Altimetry-derived Upper Ocean Thermal Structure in the Western North Pacific Ocean for Typhoon Intensity Forecast. *IEEE Trans. Geosci. Remote Sens.* 45(6), 1616-1630.
- Qiu, B., 1999: Seasonal eddy field modulation of the North Pacific Subtropical Countercurrent: TOPEX/Poseidon observations and theory. *J. Phys. Oceanogr.*, 29, 1670–1685.
- Schade, L. R., and K. A. Emanuel, 1999: The ocean's effect on the intensity of tropical cyclones: Results from a simple coupled atmosphere-ocean model. *J. Atmos. Sci.*, 56, 642-651.
- Scharroo, R., W. H. F. Smith, and J. L. Lillibridge, 2005: Satellite Altimetry and the Intensification of Hurricane Katrina. *EOS, Trans. Amer. Geophys. Union*, 86, 366-367.

- Shay, L. K., P. G. Black, A. J. Mariano, J. D. Hawkins, and R. L. Elsberry, 1992: Upper ocean response to hurricane Gilbert. *J. Geophys. Res.*, 12, 20277-20248.
- Shay, L. K., G. J. Goni, and P. G. Black, 2000: Effects of a warm oceanic feature on Hurricane Opal. *Mon. Wea. Rev.*, 128, 1366–1383.
- Siswanto, E., J. Ishizaka, K. Yokouchi, K. Tanaka, and C. K. Tan, 2007: Estimation of interannual and interdecadal variations of typhoon-induced primary production: A case study for the outer shelf of the East China Sea. *Geophys. Res. Lett.*, 34, L03604, doi:10.1029/2006GL028368.
- Stramma, L., P. Cornillon, and J. F. Price, 1986: Satellite observations of sea surface cooling by hurricanes. *J. Geophys. Res.*, 91, 5031-5035.
- Uz, B. M., J. A. Yoder, and V. Osychny, 2001: Pumping of nutrients to ocean surface waters by the action of propagating planetary waves. *Nature*, 409, 597– 600.
- Wallace, J. M., T. P. Mitchell, and C. Deser, 1989:, The influence of sea surface temperature on surface wind in the eastern equatorial Pacific: Seasonal and interannual variability. *J. Climate*, 2, 1492–1499.
- Wentz, F. J., C. Gentemann, D. Smith and D. Chelton, 2000: Satellite measurements of sea surface temperature through clouds. *Science*, 288, 5467, 847-850.
- Wu, C. C., C. Y. Lee, and I. I. Lin, 2007: The Effect of the Ocean Eddy on Tropical Cyclone Intensity. *J. Atmos. Sci.* (accepted)
- Xie, S. P., M. Ishiwatari, H. Hashizume, and K. Takeuchi, 1998: Coupled ocean-atmospheric waves on the equatorial front. *J. Geophys. Res. Lett.*, 25, 3863–3966.
- Zhu, T., and D. L. Zhang, 2006: The impact of the storm-induced SST cooling on hurricane intensity. *Advances in Atmospheric Sciences*, 23, 1, 14-22.

Figure 1: The pre-Maemi SSHA map (based on the 30 Aug–8 Sep 2003 cycle of TOPEX/Poseidon and Jason-1 measurements) showing the warm ocean eddy (characterized by positive SSHA of 10–45cm). Maemi’s track, intensity (in Saffir–Simpson scale, illustrated as color bullets) and radius of maximum wind are also shown. The storm position is denoted every 6 h. (after Lin et al., 2005).

Figure 2: Results of the CHIPS runs showing the 2 primary experiments, i.e., CTRL (a controlled run using standard CHIPS input) and EDDY (a run incorporating the warm ocean eddy information in SSHA). JTWC’s best track intensity is shown in black. (a) The intensity (m s^{-1}) evolution. (b) The typhoon-induced sea surface temperature anomaly at the storm center. (after Lin et al., 2005).

Figure 3: Ocean’s depth-temperature profiles (based on the US Naval Research Lab’s NPACNFS ocean model, Ko et al., 2003) in the warm ocean eddy and the reference background region. (after Lin et al., 2005).

Figure 4: SeaWiFS surface Chl-a image composite on (a) 27 June–4 July 2000 (before Kai-Tak); and (b) 12,14,15 July 2000 (after Kai-Tak). The circle denotes Kai-Tak’s radius of intense wind (define as 14 ms^{-1} in this work). The location of the transect tr1 crossing the longitude is also depicted. (c) Comparison of the surface Chl-a distribution along tr1; pink: before (from Figure 4a); green: after (from Figure 4b); blue: The 3-year (1998, 1999, 2001) average of surface Chl-a concentration for the month of July.

Figure 5: Same as Fig. 4 but for the TRMM TMI/SST image on (a) 1–3 July 2000 (before Kai-Tak); (b) 9 July 2000 (after Kai-Tak) (c) Comparison of the SST distribution along tr1, pink: before (from Figure 5a); brown: 1-day after (from Figure 5b); green: 4-6 days after (image

not shown); blue: The 3-year (1998, 1999, 2001) average of SST for the month of July.

Figure 6: Changes in SST (blue), surface Chl-a (green, log scale), and IPP (red) of the bloom patch before and after Kai-Tak's passage (5–8 July).

Figure 7: Sequence of representative TMI/SST images showing the evolution of Kai-Tak typhoon's cold SST patch. (a) before typhoon on 2 July 2000; (b) after typhoon on 11 July at 0100 UTC; (c) at 0900 UTC on 11 July; (d) composite of 13 and 14 July passes; (e) on 19 July. The trajectory of Kai-Tak is depicted in Figure 7b.

Figure 8. Same as Figure 7, but for the matching QuikSCAT wind speed image. (a) before typhoon on 1 and 2 July; (b) after typhoon on 10 July; (c) on 11 July; (d) on 13 July; (e) on 19 July.

Table caption:

Table 1: Comparison of the intensification parameters based on coupled model results for Maemi (2003), Opal (1995), Bret (1999), and Mitch (1998).

Figure 1

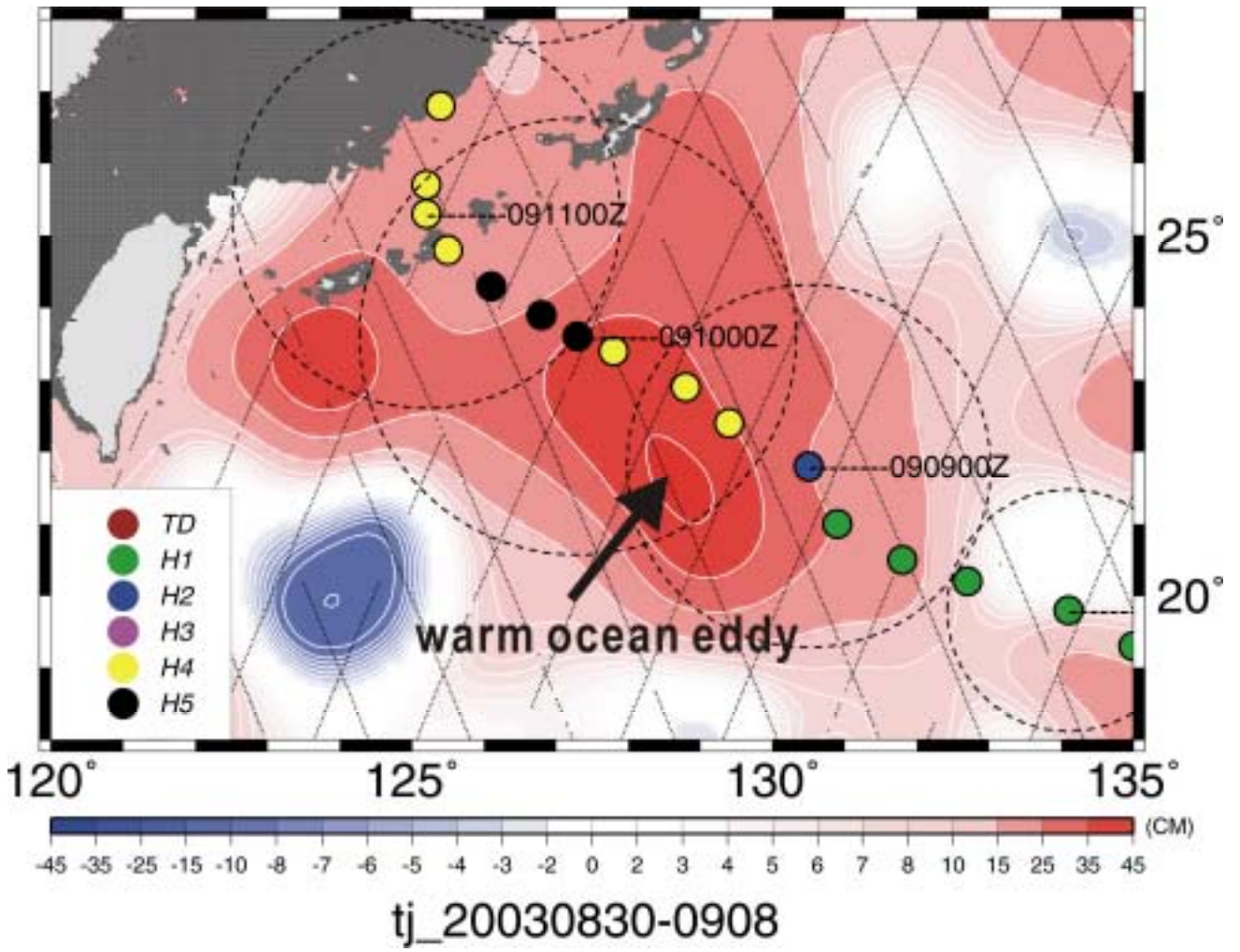


Figure 2

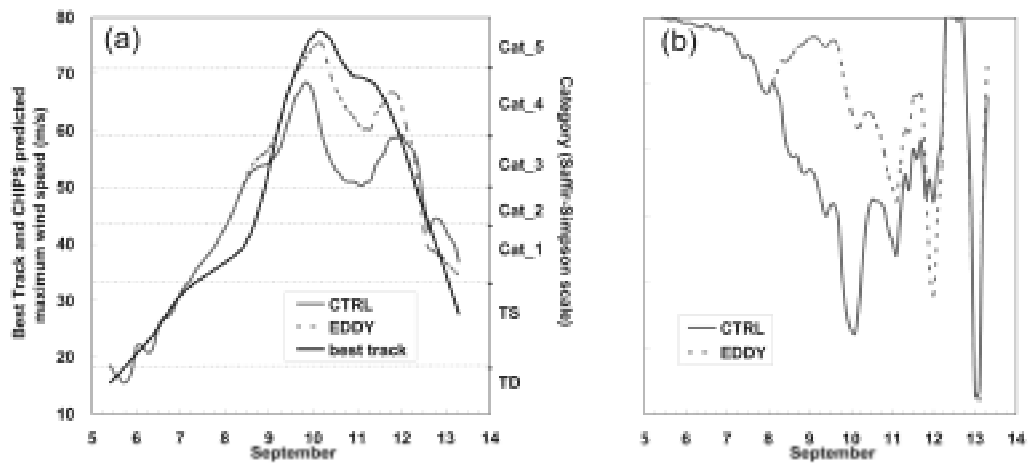


Figure 3

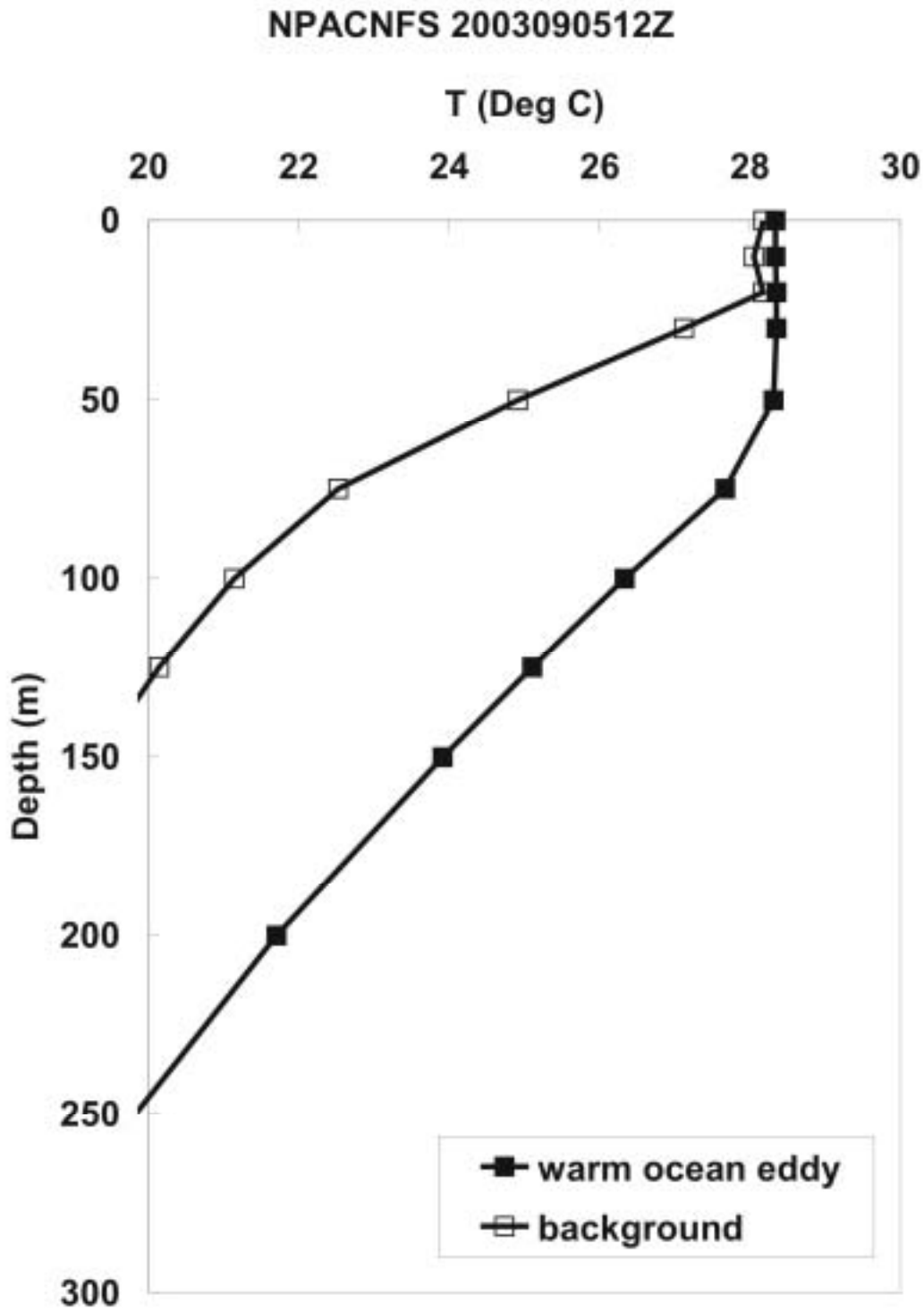


Figure 4

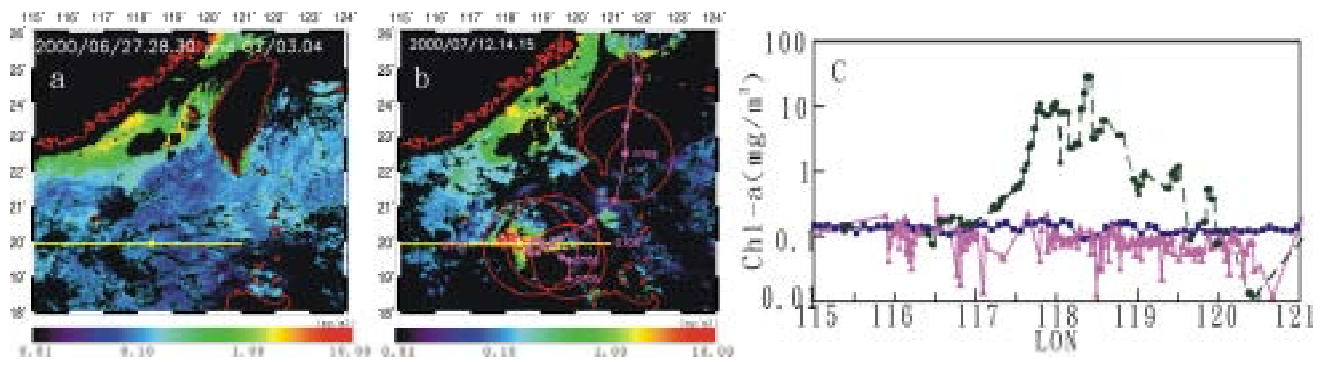


Figure 5

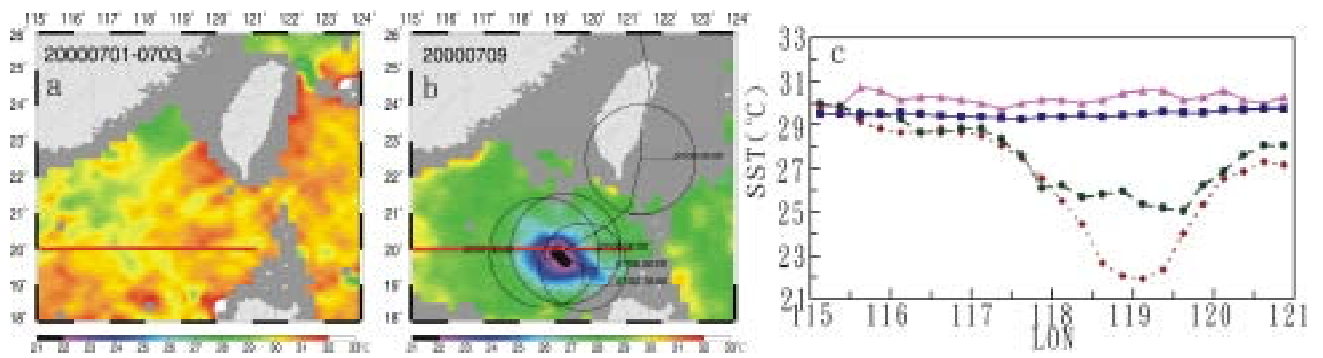


Figure 6

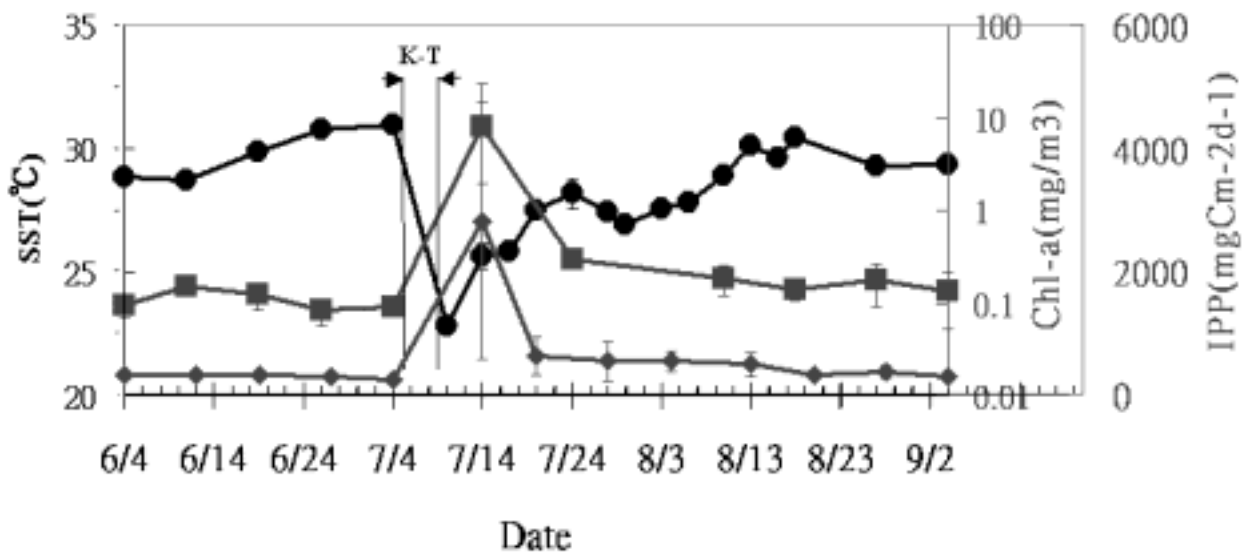


Figure 7

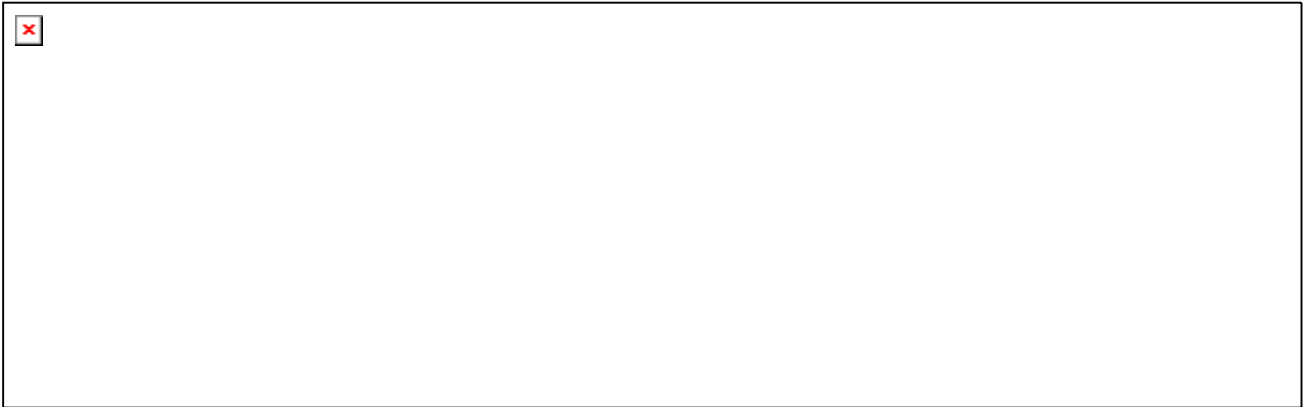


Figure 8

